Journal of Alloys and Compounds 495 (2010) 299–304

Contents lists available at ScienceDirect

Journal of Alloys and Compounds

journal homepage: www.elsevier.com/locate/jallcom

Phase separation in Ni–Nb–Y metallic glasses

Norbert Mattern[a,*], Thomas Gemming[a], Jürgen Thomas[a], Günter Goerigk[b], Hermann Franz[c], Jürgen Eckert[a,d]

[a] Leibniz-Institute IFW Dresden, Institute for Complex Materials, P.O. Box 270116, D-01171 Dresden, Germany
[b] Institute for Solid State Research, FZ Jülich, P.O. Box 1913, D-52425 Jülich, Germany
[c] HASYLAB at DESY, Notkestr. 85, D-22603 Hamburg, Germany
[d] TU Dresden, Institute of Materials Science, D-01062 Dresden, Germany

ARTICLE INFO

Article history:
Received 31 July 2008
Received in revised form 5 October 2009
Accepted 6 October 2009
Available online 13 October 2009

Keywords:
Metallic glasses
Phase separation
Spinodal decomposition
Small angle X-ray scattering

ABSTRACT

The ternary system Ni–Nb–Y exhibits an extended miscibility gap in the equilibrium liquid. The decomposition of the liquid can be used to prepare phase-separated Ni–Nb–Y glasses by means of rapid quenching of the melt. Phase separation and structure formation take place during quenching in the undercooled liquid. The temperature dependence of the critical temperature of liquid–liquid phase separation T_C determines essentially the quenched in microstructures. For Ni contents <60 at.% coarsened hierarchical microstructures of two-phase glasses are formed. For Ni contents >60 at.% early stages of decomposition are obtained with correlation lengths in the nanometer-range. In situ small angle X-ray scattering at elevated temperatures gives evidence of the spinodal character of the decomposition.

1. Introduction

Phase separation in metallic glasses was reported already many years ago for some metallic glasses [1–6]. Recent reinvestigation did not confirm the old findings [7–9]. Metallic glasses are usually composed of elements with strong negative enthalpy of mixing ΔH_{mix} between the main constituents which is related to the glass forming ability, compound formation and the presence of deep eutectics [10,11]. At least most glassy alloys with $\Delta H_{mix} \ll 0$ are homogeneous, and phase separation seems to be exceptional. On the other side, recent development of bulk metallic glasses (BMGs) led to new phase-separated metallic glasses [12–18] by introducing element additions having strong positive enthalpy of mixing ($\Delta H_{mix} \gg 0$) to one of the main constituent. The first phase-separated metallic glass was probably prepared in the Zr–Y–Al–Ni system by Inoue et al. [12]. In 2004 Kündig et al. initiated the use of element additions with $\Delta H_{mix} \gg 0$ as concept to prepare a two-phase glassy alloys in the Zr–La–Al–Ni–Cu system [13]. In the following years, phase-separated metallic glasses were successfully prepared in several alloy systems, like Zr–Y–Co–Al [14], Ni–Nb–Y [15], Zr–Nd–Al–Co [16], Cu–(Zr,Hf)–(Gd,Y)–Al [17], and Zr–(Ce,Pr,Nd)–Al–Ni [18]. In all these cases, the alloy consists of elements combining high glass forming ability with demixing tendency by adding an element having strong positive enthalpy of mixing to one of the main constituent. Liquid–liquid phase separation leads to a special microstructure with a length-scale up to several micron with features of self-similarity as observed by transmission electron microscopy [13,19,20]. In general, the formed microstructures depend on the thermodynamic properties of the alloy system as well as on preparation conditions like the cooling rate or casting temperature. In this paper we analyze the relationship between composition dependent thermodynamic properties and the structure formation of rapidly quenched Ni–Nb–Y alloys.

2. Experimental

Pre-alloyed ingots were prepared by arc-melting elemental Ni, Nb and Y with purities of 99.9% or higher in a Ti-gettered argon atmosphere. To ensure homogeneity, the samples were remelted several times. From these pre-alloys, ribbons (3 mm in width and 30 μm in thickness) with nominal compositions $Ni_{54}Nb_{23}Y_{23}$, and $Ni_{70}Nb_{15}Y_{15}$ were prepared by single-roller melt spinning under argon atmosphere. Chemical compositions were analyzed by the titration technique. The determined values were $Ni_{54.9}Nb_{25.0}Y_{20.1}$ and $Ni_{71.3}Nb_{13.7}Y_{15.0}$, respectively. The casting temperature was 1923 K. High energy X-ray diffraction (XRD) experiments were conducted at the synchrotron beam-line BW5 at HASYLAB, Hamburg. Intensities were recorded in transmission geometry by a Ge-point detector using a wavelength of λ = 0.01250 nm. Transmission electron microscopy (TEM) was performed with a FEI Tecnai F30 electron microscope. For the TEM investigations, the ribbons were thinned by Ar ion milling at an accelerating voltage of 2.5 keV under a grazing incidence angle of 4°. Anomalous small angle X-ray scattering (ASAXS) was measured with the JUSIFA beam-line at the DORIS storage ring at HASYLAB/DESY Hamburg. The measurements were performed in the vicinity of the K-absorption edge of Ni at 8333 eV. A heating stage under vacuum was used for in situ SAXS measurements. Patterns were recorded 15 min isothermally at elevated temperatures with a repetition each 30 min.

* Corresponding author. Tel.: +49 3514659467; fax: +49 3514659452.
E-mail address: n.mattern@ifw-dresden.de (N. Mattern).

0925-8388/$ – see front matter © 2009 Elsevier B.V. All rights reserved.
doi:10.1016/j.jallcom.2009.10.013

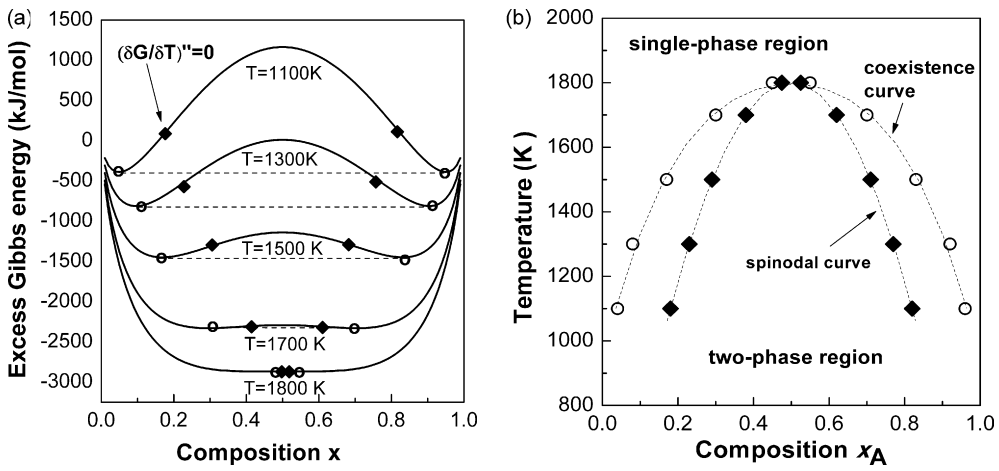

Fig. 1. (a) Excess free energy ΔG_{excess} of a binary liquid AB (ΔH_{mix} = +30 kJ/mol) versus temperature and (b) corresponding phase diagram with miscibility gap.

3. Thermodynamics of phase separation

Phase separation in the equilibrium liquid occurs in about 10% of the reported binary phase diagrams [21]. In the case of strong positive enthalpy of mixing between the constituents unlike atoms avoid compound formation in the solid as well as in the liquid state. The phase equilibrium is determined by the minimum of the Gibbs energy $G = H - TS$. Binary solution phases, such as liquid and disordered solid solutions of type A_xB_{1-x}, can be described by the regular-solution type model. The Gibbs energy is a composition weighted sum of the components plus an excess part of mixing:

$$G = x_A G_A + x_B G + R \cdot T \cdot [x_A \ln(x_A) + x_B \ln(x_B)] + \Delta G_{excess}, \quad (1)$$

where x_A, x_B are the molar fractions of elements A and B, R is the gas constant, and T is temperature in Kelvin. The extra energy of mixing ΔG_{excess} is described via interaction parameters ${}^{i}L^{\varphi}_{A,B}(T)$ as:

$$\Delta G_{excess} = x_A \cdot x_B \cdot \sum {}^{i}L^{\varphi}_{A,B}(T) \cdot (x_A - x_B)^i \quad (2)$$

Fig. 1a shows the excess part ΔG_{excess} assuming only zero-order parameter with ${}^{0}L^{\varphi}_{A,B}(T) = \Delta H_{mix} = +30$ kJ/mol. The positive interaction parameter results in the double minimum shape of the free energy versus composition. For any composition between the two minima, the alloy lowers the free energy by separating into two phases. With increasing temperature the entropic part of mixing lead to a reduction of the composition difference between the two phases and above the critical temperature the alloy becomes homogeneous. From the temperature dependence of the free energy curves, the phase diagram shown in Fig. 1 can be constructed with a miscibility gap below the critical point (T_C, $c^{crit.}$). The composition dependence of the free energy can be distinguished: states where $(\delta G/\delta c)'' > 0$ are called metastable, and states where $(\delta G/\delta c)'' < 0$ are called unstable. The locus of inflection points $(\delta G/\delta c)'' = 0$ defines the spinodal curve. According to Cahn–Hilliard–Cook theory, this distinction is linked to different transformation mechanism [22]. In the unstable regime, statistical fluctuations spontaneously grow to an extended concentration wave with a correlation length ζ. In the metastable regime locally decomposition starts by nucleation which means large-amplitude fluctuations are formed in order to start the transformation.

Fig. 2 shows schematically the structure formation of a melt with a miscibility gap upon cooling. Reaching the critical temperature, the melt becomes unstable. In the spinodal regime the decomposition is initiated via the spontaneous formation and subsequent growth of coherent composition fluctuations (spinodal decomposition). At later stages the stationary state of the composition amplitude is reached and the composition profile may change into a square-like shape. Further cooling (or longer time) leads to coarsening of the microstructure due to diffusion and coalescence. The flow in the liquid leads to a coalescence of the droplets to larger domains. Hydrodynamical flow, driven by the pressure difference between points of different curvature at the domains, leads to a reduction of the interface length, and as a consequence to a more spherical shape of the domains. Secondary decomposition within the melt may take place if the diffusivity is too low to reach its equilibrium composition at each temperature during cooling. Depending on the difference in mass density the two melts may separate into two layers. Upon further cooling than the two melts crystallize independently at different temperatures. If the glass forming ability is high and the cooling rate is sufficient, the phase-separated undercooled liquids transform into glasses at the corresponding glass transition temperatures.

4. Phase separation in liquid and glassy Ni–Nb–Y alloys

Fig. 3a shows the calculated binary Nb–Y phase diagram (CALPHAD method), which is characterized by complete decomposition into the terminal phases Nb and Y in the solid state and by a miscibility gap in the liquid state with a monotectic temperature T_{mono} = 2675 K, and critical temperature T_{crit} of about 3000 K, respectively [23]. The miscibility gap in the liquid of the binary system extends into the ternary Ni–Nb–Y system up to a high

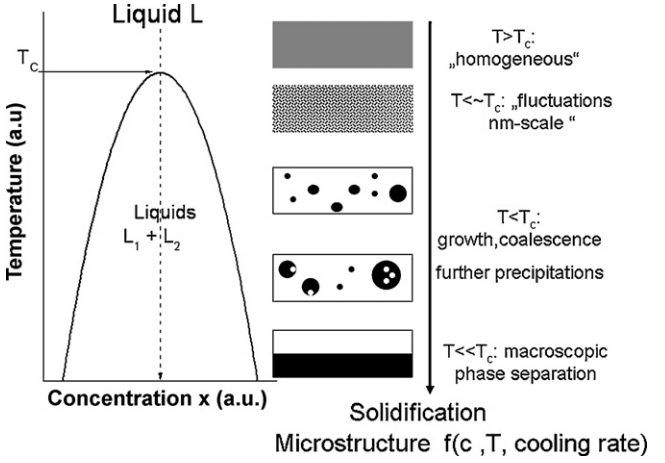

Fig. 2. Schematic representation of the structure formation during cooling a phase separating liquid.

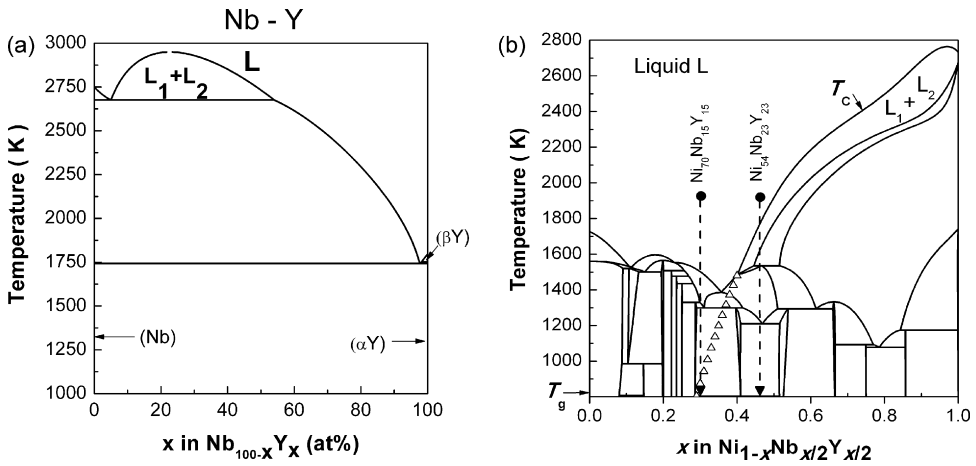

Fig. 3. Calculated phase diagrams (a) binary Nb–Y, (b) pseudo-binary section Ni–$Nb_{50}Y_{50}$ of the ternary Ni–Nb–Y system.

Ni content as shown in Fig. 3b by the pseudo-binary section Ni–$Nb_{50}Y_{50}$. With increasing Ni content, the monotectic temperature and the critical temperature are lowered. The extrapolation of the critical temperature T_C for Ni content >60 at.% (metastable undercooled liquid) is also depicted by the triangles in Fig. 3b.

The phase separation of Ni–Nb–Y alloys in the liquid state leads to a particular microstructure of the cast samples. Fig. 4 shows the SEM images of a $Ni_{54}Nb_{23}Y_{23}$ alloy obtained for different casting conditions (Fig. 4a and b cast on a copper plate, Fig. 4c melt spun ribbon). Coarse microstructure with grey deformed spheres (NiNb-rich) in the dark matrix gives clear evidence of the phase separation of the liquid at T = 1573 K (Fig. 4a) which is below the critical temperature T_C = 1770 K of the alloy. Casting under the same conditions from T = 1973K which is above T_C leads to a finer microstructure (Fig. 4b). Decomposition and growth of the liquids take place during casting. The size of the liquid droplets varies between contact side (bottom) and free surface (top) of the sample as a consequence of the gradient of the cooling rate. Rapid quenching of $Ni_{54}Nb_{23}Y_{23}$ by melt spinning reduces the size of the inhomogeneities furthermore by three orders of magnitude (Fig. 4c). Fig. 5 shows the microstructure in more detail by the TEM image. An inhomogeneous spherical microstructure is visible with a sharp interface between precipitates and matrix. Local electron diffraction and high resolution TEM proved an amorphous structure for both regions. The contrast in the TEM image is related to local differences in chemical compositions, as measured by energy dispersive X-ray analysis (EDX). The spherical dark precipitates are Nb-enriched with an average composition of $Ni_{50}Nb_{44}Y_6$, and the grey matrix phase is Y-enriched with an average composition of $Ni_{58}Nb_7Y_{35}$, respectively. Both are not single phase regions. We observe a distribution in size with some features of self-similarity. Y-enriched precipitations exist inside the Nb-enriched spheres, and the grey matrix contains Nb-rich precipitates, which are visible down to a size of <10 nm. Similar microstructures were reported in the literature [13–20] also for other phase-separated glassy alloys.

XRD measurements also confirm the glassy state of the two-phase structure. Fig. 6a shows the structure factor $S(q)$ of the $Ni_{54}Nb_{23}Y_{23}$ two-phase metallic glass as calculated from the XRD diffraction data. The first diffuse maximum of $S(q)$ exhibits a shoulder on the low-q side due to the superposition of the scattering intensities of the two amorphous phases, also seen in the electron diffraction of the TEM (Fig. 5, inset). We also measured the struc-

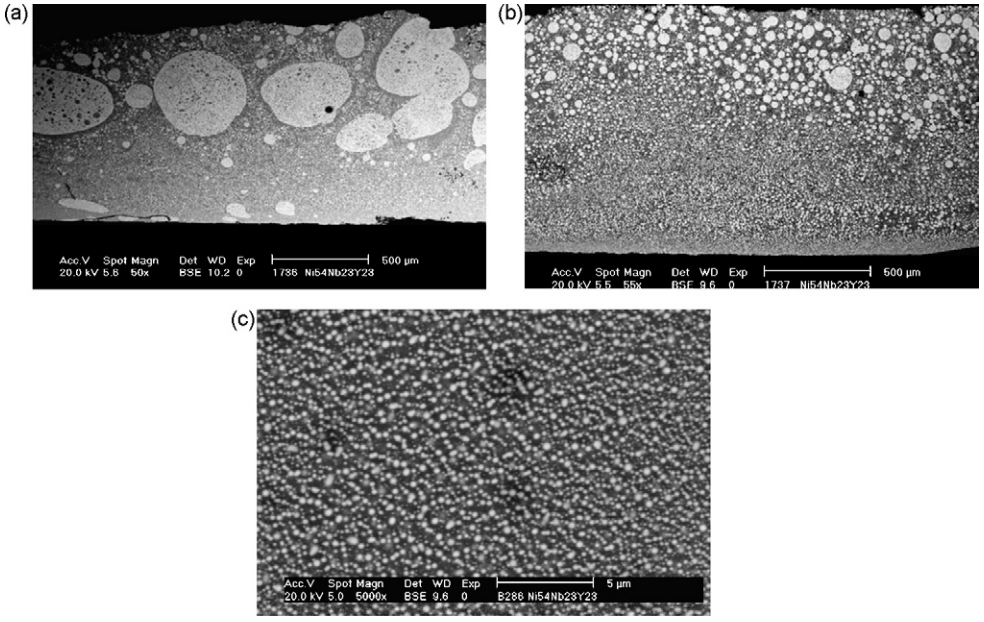

Fig. 4. SEM images of $Ni_{54}Nb_{23}Y_{23}$ (a) cast from T = 1573 K, (b) cast from T = 1773 K, and (c) rapidly quenched from 1923 K.

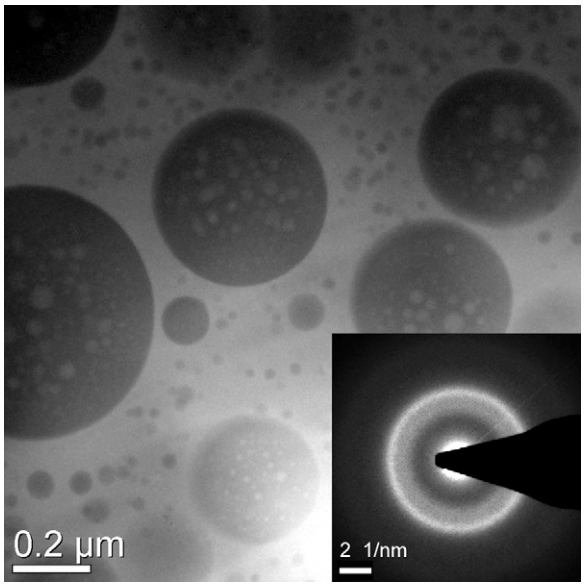

Fig. 5. TEM bright field images and electron diffraction patterns of $Ni_{54}Nb_{23}Y_{23}$ glass rapidly quenched from 1923 K.

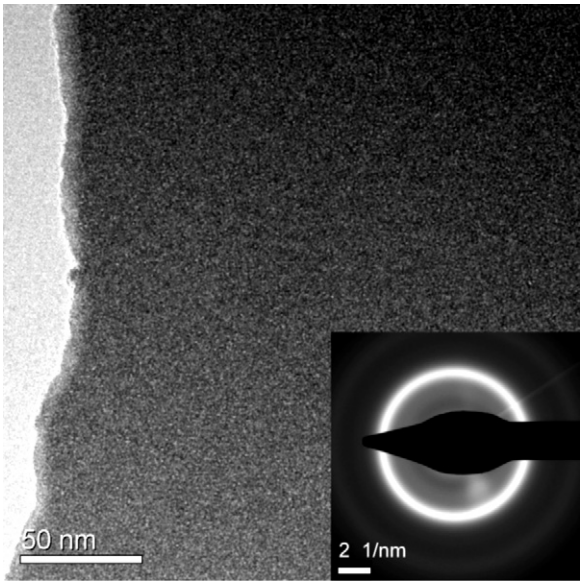

Fig. 7. TEM bright field images and electron diffraction patterns of $Ni_{70}Nb_{15}Y_{15}$ (rapidly quenched from 1923 K).

ture factors of rapidly quenched amorphous $Ni_{50}Nb_{50}$ and $Ni_{58}Y_{42}$ as single phase references for the two-phase glass. Fig. 6a compares the averaged sum of the structure factors of the two binary amorphous phases with the measured curve. The calculation agrees well with the experimental data.

From the structure factors the atomic pair correlation functions $g(r) = \rho(r)/\rho_0$ were calculated by the Fourier transform of $S(q)$. For all alloys, the first maximum of $g(r)$ consists of several components corresponding to the weighted partial atomic pair correlations. In the binary $Ni_{58}Y_{42}$ alloy three maxima exist which can be attributed to the nickel–nickel (r^1_{Ni-Ni}), nickel–yttrium (r^1_{Ni-Y}) and to the yttrium–yttrium (r^1_{Y-Y}) nearest neighbour distances. For the binary $Ni_{50}Nb_{50}$ glass the individual contribution are not resolved. The weighted sum of the $g(r)$ curves of the two binary glasses is in a good agreement with the experimental data of the ternary $Ni_{54}Nb_{23}Y_{23}$ two-phase metallic glass (Fig. 6b). The distance $r^1_{Y-Y} = 0.355$ nm is well separated in the binary as well as in the ternary alloy due to the larger atomic diameter of yttrium (0.364 nm) compared to that of niobium (0.286 nm).

In contrast to the quenched metallic glasses with extended heterogeneities, the microstructure becomes different for Ni–Nb–Y glasses having a Ni content >60 at.%. Fig. 7 shows the microstructure of the rapidly quenched $Ni_{70}Nb_{15}Y_{15}$ alloy. The bright field TEM images points to an almost homogeneous microstructure. The amorphous structure is confirmed by high resolution TEM and local electron diffraction (inset Fig. 7). The XRD pattern and thermal behaviour (not shown here) also indicates the glassy state for as-quenched $Ni_{70}Nb_{15}Y_{15}$ ribbon. To check whether the microstructure is really homogeneous, X-ray small angle scattering (SAXS) was measured. This method provides integral information on existing inhomogeneities in electron density with a size ranging from the nanometer up to the micron range [24]. The calibrated SAXS curves $d\sigma/d\Omega(q)$ (q is the magnitude of the scattering vector, $q = 4\pi \sin\theta/\lambda$, scattering angle 2θ, wavelength λ) depend on differences in electron density, but also on the volume fraction, size, and shape of the inhomogeneities built up from the different phases [24]:

$$\frac{d\sigma}{d\Omega}(\vec{q}) = \int \tilde{\rho}^2(\vec{r})\ \exp(i\vec{q}\vec{r}) d^3r, \tag{3}$$

where $\tilde{\rho}^2(\vec{r})$ represents the so-called auto-correlation function, which is calculated from the spatial distribution of the electron

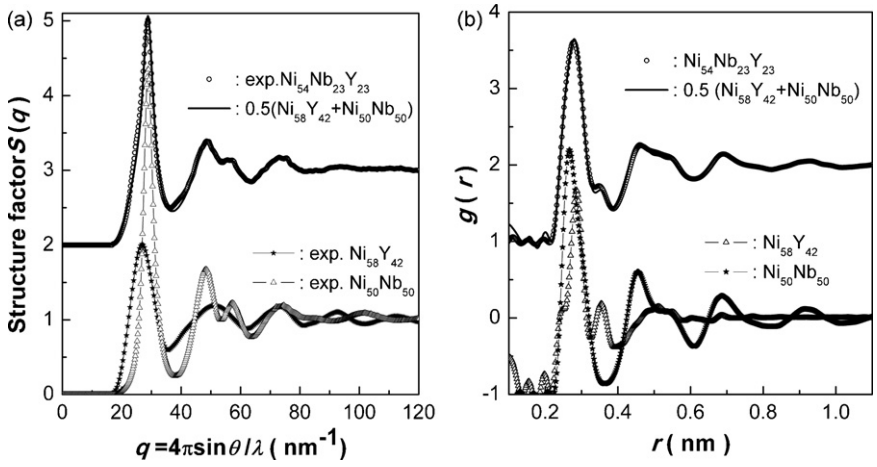

Fig. 6. (a) Structure factor of rapidly quenched $Ni_{54}Nb_{23}Y_{23}$ in comparison with those of binary NiY and NiNb glasses and (b) corresponding atomic pair correlation functions $g(r)$.

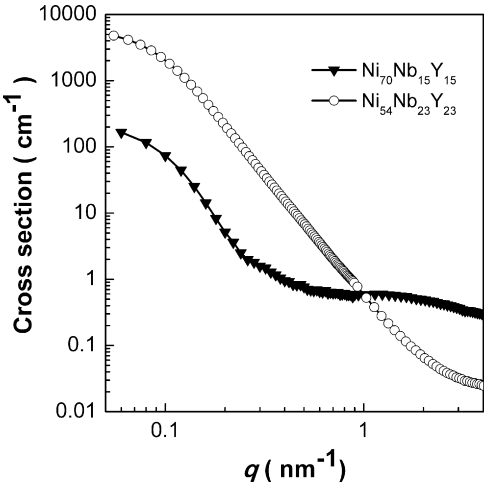

Fig. 8. SAXS curves $d\sigma/d\Omega(q)$ of glassy Ni–Nb–Y alloys.

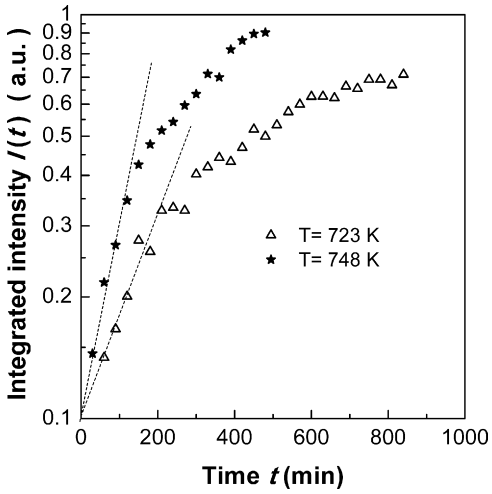

Fig. 10. Integral intensity of the maximum of the SAXS curves at elevated temperatures versus time.

scattering-length density $\rho(r)$. The scattering length can be tuned by variation of the energy at the X-ray absorption edges of the involved elements which is explored for anomalous small angle X-ray scattering (ASAXS) [25]. In the case of an isotropic structure, the scattering curves averaged over all orientations are given by [24]:

$$\frac{d\sigma}{d\Omega}(q) = \int 4\pi \cdot r^2 \tilde{\eta}^2(r) \frac{\sin(qr)}{qr}\, dr, \tag{4}$$

where $\tilde{\eta}^2(r) = \tilde{\rho}(r)^2 - V\rho_0^2$ is the square of the so-called electron density fluctuation $\eta(r) = \rho(r) - \rho_0$, which is calculated from the difference of the electron scattering-length density $\rho(r)$ and the average electron scattering-length density ρ_0 in the sample volume V. The SAXS curves $d\sigma/d\Omega(q)$ of the two samples measured at the energy $E = 8291$ eV, 42 eV below the Ni–K edge are shown in Fig. 8. For the rapidly quenched $Ni_{54}Nb_{23}Y_{23}$ the strong SAXS intensities clearly reflect the presence of chemical inhomogeneities in the samples. The slope in the linear range (of $\log(I)$ versus $\log(q)$), $p = -3.7$, points to a polydisperse microstructure. The polydisperse character of the microstructure (also seen in the TEM image Fig. 5) is a result of the structure formation during quenching (Fig. 2). In contrast, the $Ni_{70}Nb_{15}Y_{15}$ glass show weak contribution in the SAXS data for $q > 0.2\ nm^{-1}$. The curve give evidence for the existence of correlated fluctuations in electron density for the Ni–Nb–Y alloys by the maximum at $q = 1.2\ nm^{-1}$. Using the rough relationship between correlation length ζ in real space and peak maximum q_{max} in reciprocal distances $\zeta = 2\pi/q_{max}$ one obtains $\zeta = 5$ nm for the $Ni_{70}Nb_{15}Y_{15}$ glassy alloy.

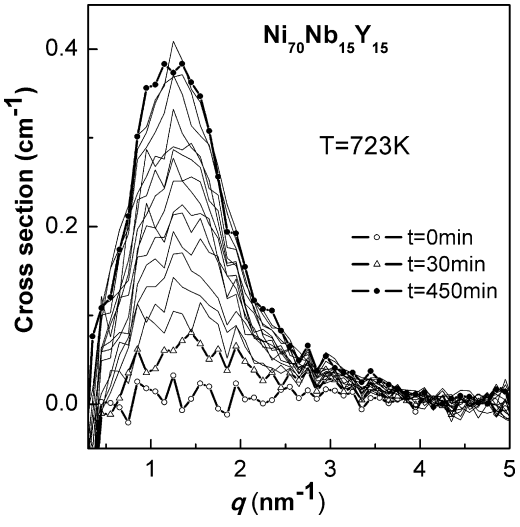

Fig. 9. In situ SAXS $d\sigma/d\Omega(q)$ of $Ni_{70}Nb_{15}Y_{15}$ glass at $T = 723$ K repeatedly recorded each 30 min up to 450 min.

In order to analyze the behaviour of the decomposition in the undercooled liquid state, in situ ASAXS measurements were performed at elevated temperatures. In situ patterns recorded during isothermal annealing at $T = 723$ K are shown in Fig. 9. With increasing time, the height or integral intensity of the maximum of the ASAXS curve enlarges. The maximum position $q_{max} = 1.2\ nm^{-1}$ remains unchanged during the heat treatment. A similar behaviour is observed for another sample measured at $T = 748$ K. The integral intensities of the SAXS curves as a function of time are shown in Fig. 10. It can be seen from the semi-logarithmic plot that the intensity increases linear for the early stages. At later stages the growth diminishes and converges to a stationary stage. Both SAXS curves can be transformed into each other by a scaling factor describing the same thermally activated process of decomposition. The retention of the amorphous state of the samples during heat treatment was proven by subsequent XRD measurements of the annealed samples.

5. Discussion

The microstructure formation during rapid quenching of Ni–Nb–Y liquids is related to the phase diagram and especially to the phase separation in the undercooled melt. As shown in Fig. 3b the critical temperature T_C decreases with increasing Ni content. For rapidly quenched $Ni_{54}Nb_{23}Y_{23}$ the microstructure represents a coarsened state of spinodal decomposition, growth of the melts, and secondary decomposition within the liquids (Fig. 2). For the alloys with higher Ni content, the phase separation proceeds in the metastable undercooled liquid at much lower temperatures. Lower temperature means slower kinetics of decomposition and growth after the phase separation. Furthermore, less time is required to reach the glass transition temperature T_g where the undercooled liquids become frozen into the glass. So, early stages of decomposition can be obtained by rapid quenching.

The structure formation by spinodal decomposition is usually described by the Cahn–Hilliard theory [22]. The decomposition is initiated via the spontaneous formation and subsequent growth of coherent composition fluctuations. Using Eq. (4) the ASAXS intensity was calculated for a concentration fluctuation $c(r) = A\cos(1.26r)$ as a function of the amplitude A at a constant fluctuation length

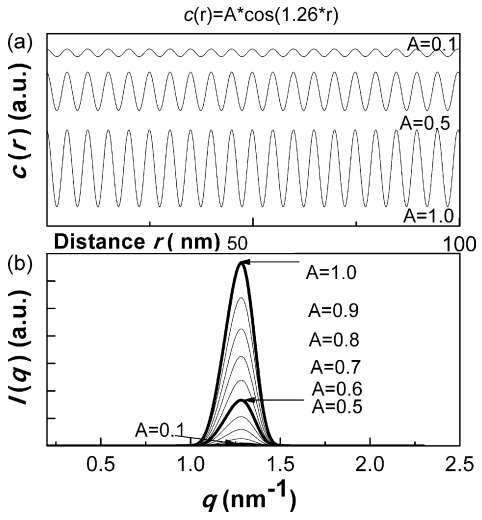

Fig. 11. (a) Concentration fluctuation $c(r)$ and (b) corresponding SAXS intensity $I(q)$ as function of amplitude A.

of 5 nm. The corresponding $I(q)$ curves with an increasing intensity of the maximum at about 1.2 nm^{-1} are shown in Fig. 11. In the calculated scattering curves as well as in the experimental SAXS data (Fig. 9), the position of the maximum of $I(q)$ does not change. This means that for the $Ni_{70}Nb_{15}Y_{15}$ glass the fluctuation length remains constant during the decomposition process. The linear Cahn–Hilliard theory gives an exponential time dependence for the scattered intensity [22]. This in agreement with the experimentally observed dependence of $I(q)$ of early stages during annealing of the $Ni_{70}Nb_{15}Y_{15}$ glass. At later stages the stationary state of the amplitude is reached and composition profile may change into a square-like shape which gives reason for the deviation from the exponential growth of the SAXS intensity. The constant correlation length as well as the exponential increase of the intensity with time point to spinodal decomposition mechanism in the supercooled state of $Ni_{70}Nb_{15}Y_{15}$ glass.

6. Conclusions

In alloy systems with strong positive enthalpy of mixing between the main components a miscibility gap may occur in the equilibrium liquid, or in the metastable undercooled liquid, respectively. For the ternary Ni–Nb–Y system an extended miscibility gap exists in the equilibrium liquid. Due to high glass forming ability, phase-separated Ni–Nb–Y metallic glasses can be prepared by rapid quenching of the melt. The temperature dependence of the critical temperature of liquid–liquid phase separation T_C determines essentially the formed microstructures. For high Ni contents early stages of decomposition are obtained. In situ small angle X-ray scattering at elevated temperatures gives evidence of the spinodal character of the decomposition. Liquid–liquid phase separation can be used as a concept to prepare new phase-separated metallic glasses with particular microstructures not possible by other methods.

Acknowledgement

Financial support of the Deutsche Forschungsgemeinschaft DFG (project Ma1531/10-1) is gratefully acknowledged.

References

[1] H.S. Chen, D. Turnbull, Acta Metall. 17 (1969) 1021.
[2] H.S. Chen, Mater. Sci. Eng. 23 (1976) 151.
[3] L.E. Tanner, R. Ray, Scripta Mater. 14 (1980) 657.
[4] T.W. Barbee, R.G. Walmsley, A.F. Marshall, D.L. Keith, D.A. Stevenson, Appl. Phys. Lett. 38 (1981) 132.
[5] D. Deng, A.S. Argon, Acta Metall. 34 (1986) 2011.
[6] H.U. Krebs, D.J. Webb, A.F. Marshall, Phys. Rev. B 35 (1987) 5392.
[7] D. Nagahama, T. Ohkubo, K. Hono, Scripta Mater. 49 (2003) 729.
[8] K. Kajiwara, M. Ohnuma, T. Ohkubo, D.H. Ping, K. Hono, J. Mater. Sci. Eng. A375–377 (2004) 738.
[9] S.V. Magde, R. Rösner, G. Wilde, Scripta Mater. 53 (2005) 1147.
[10] A. Inoue, Mater. Trans. 43 (2002) 1892.
[11] W.L. Johnson, MRS Bull. 24 (1999) 42.
[12] A. Inoue, S. Chen, T. Masumoto, Mater. Sci. Eng. A 179/180 (1994) 346.
[13] A.A. Kündig, M. Ohnuma, D.H. Ping, T. Ohkubo, K. Hono, Acta Mater. 52 (2004) 2441.
[14] B.J. Park, H.J. Chang, D.H. Kim, W.T. Kim, Appl. Phys. Lett. 85 (2004) 6353.
[15] N. Mattern, U. Kühn, A. Gebert, T. Gemming, M. Zinkevich, H. Wendrock, L. Schultz, Scripta Mater. 53 (2005) 271.
[16] E.S. Park, E.Y. Jeong, J.K. Lee, A.R. Kwon, A. Gebert, L. Schultz, H.J. Chang, D.H. Kim, Scripta Mater. 56 (2007) 197.
[17] E.S. Park, J.S. Kyeong, D.H. Kim, Scripta Mater. 57 (2007) 49.
[18] T. Wada, D. Louzguine-Luzgin, A. Inoue, Scripta Mater. 57 (2007) 901.
[19] B.J. Park, H.J. Chang, D.H. Kim, W.T. Kim, K. Chattopadhyay, T.A. Abindanan, S. Bhattacharyya, Phys. Rev. Lett. 6 (2006) 245503.
[20] N. Mattern, T. Gemming, G. Goerigk, J. Eckert, Scripta Mater. 57 (2007) 29.
[21] T.B. Massalski, P.R. Subramanian, H. Okamoto, L. Kacprzak (Eds.), Binary Alloy Phase Diagrams, vols. 1, 2 and 3, 2nd ed., ASM International, Materials Park, OH, 1990.
[22] K. Binder, P. Fratzl, Spinodal decomposition, in: G. Kostorz (Ed.), Phase Transformations in Materials, Wiley-VHC, Weinheim, 2001, p. 409.
[23] N. Mattern, M. Zinkevich, W. Löser, G. Behr, J. Acker, J. Phase Equilib. Diff. 29 (2008) 141.
[24] O. Glatter, O. Kratky, Small-Angle X-ray Scattering, Academic Press, London, 1982.
[25] G. Goerigk, H.G. Haubold, O. Lyon, J.P. Simon, J. Appl. Cryst. 36 (2003) 425.